Article

J. Biol. Regul. Homeost. Agents. 2024; 38(6): 5045–5064
https://doi.org/10.23812/j.biol.regul.homeost.agents.20243806.402

Identification and Verification of a New Anoikis-Related Signature and Subgroups in Pancreatic Ductal Adenocarcinoma

Menghua Du[1], Jia Liu[2], Xu Lu[1,*]

[1]Department of Radiotherapy, Suzhou Ninth People's Hospital, 215200 Suzhou, Jiangsu, China
[2]Department of Radiotherapy, Jiangyin Hospital Affiliated to Nantong University, 214400 Jiangyin, Jiangsu, China
*Correspondence: dirty.6@163.com (Xu Lu)
Submitted: 25 January 2024 Revised: 5 March 2024 Accepted: 7 March 2024 Published: 1 June 2024

Background: Anoikis, a process crucial for maintaining tissue homeostasis, is implicated in tumor initiation and progression, particularly in pancreatic ductal adenocarcinoma (PDAC), known for its dismal prognosis. Understanding the molecular mechanisms underlying anoikis is imperative for unraveling PDAC pathogenesis. This study aimed to investigate the role of anoikis-related genes (ARgs) in PDAC prognosis and their interaction with the tumor immune environment.
Methods: Differential expression analysis of ARgs between tumor tissues and normal tissues was conducted utilizing The Cancer Genome Atlas (TCGA) dataset. Then, utilizing weighted gene co-expression network analysis (WGCNA) and least absolute shrinkage and selection operator (LASSO) regression analysis, ARgs with prognostic relevance were discovered as differentially expressed hub genes. Subsequently, these hub ARgs were employed to construct risk signatures, and a consensus cluster analysis was conducted. Predictive values of risk groups and molecular subtypes, alongside characteristics of tumor immune microenvironment, were analyzed to accurately predict the prognosis. Combined with risk signatures and molecular subtypes, validation of prognostic classification models was achieved through external datasets and RT-PCR experiments.
Results: We identified six hub ARgs, divided patients into two groups according to their expression as the basis of consensus cluster analysis, established an ARgs risk signature based on four of these ARgs, divided patients into high-risk and low-risk groups, and accurately predicted their prognosis. Furthermore, by combining the above classification, the two subgroups showed significant differences in their prognostic outcomes and immune microenvironment characteristics. To further validate our findings, we utilized data from the International Cancer Genome Consortium (ICGC). RT-PCR was performed to verify the expressions of hub ARgs.
Conclusion: Our findings underscore the role of anoikis in shaping the tumor microenvironment and PDAC progression. Moreover, the established risk signature and classification exhibit close associations with the immune microenvironment, showing potential for prognostic predictions in PDAC patients.

Keywords: anoikis; PDAC; tumor immune microenvironment; TCGA; ICGC; prognosis

Introduction

Pancreatic cancer, ranking seventh among the leading causes of cancer-related deaths globally, has the highest mortality rate compared to its incidence rate. In 2020 alone, there were 495,773 new patients diagnosed with this disease, resulting in 466,003 fatalities, emphasizing its profound impact on public health. With a meager 10% 5-year survival rate, it presents a formidable challenge [1–3].

Pancreatic ductal adenocarcinoma (PDAC) constitutes 90% of pancreatic cancer cases and displays significant ethnic and regional differences in incidence rates. Western Europe and North America report the highest incidence, while East Africa and South-Central Asia record the lowest, with disparities exceeding tenfold [2]. Pancreatic cancer is a complex disease stemming from a combination of genetic and non-genetic factors. Unfortunately, by the time symptoms manifest, the disease often progresses beyond operable stages, contributing significantly to its poor prognosis. Even radical resection fails to substantially improve long-term survival rates for pancreatic cancer patients [4].

The absence of an effective screening method to detect pancreatic cancer exacerbates the situation, impeding early detection efforts [5]. The Alliance for Early Detection of Pancreatic Cancer advocates for standardized imaging and MRI report templates to enhance screening consistency and accuracy [6,7]. However, relying solely on imaging approaches for early pancreatic cancer detection proves insufficient, underscoring the necessity for integrating biomarker detection. Recent studies propose various novel serum biomarkers [8–10].

Journal of
BIOLOGICAL REGULATORS
and Homeostatic Agents

Continually refining existing predictive models and exploring novel, more convenient, accurate, and personalized models are imperative. These efforts will offer valuable insights to aid in clinical decision-making processes.

Anoikis is a programmed cell death process triggered when cells lose contact with the extracellular matrix and neighboring cells [11]. Resistance to anoikis is vital for tumor cells survival during bloodstream circulation and malignant cells metastasis [12,13]. The ability to evade apoptosis and complete this process with robust anti-anoikis mechanisms renders it a significant contributing factor in tumor progression [14]. Consequently, unraveling the molecular mechanisms underpinning anoikis is crucial for developing effective cancer treatment options. Anoikis is a pivotal element in tumorigenesis, necessitating a profound understanding of its underlying molecular mechanism for the development of effective cancer treatment options. Despite extensive literature exploring the roles of anoikis-associated genes in the prognosis of various cancers [15–18], their specific impact on PDAC patients remains insufficiently elucidated. Hence, there exists a critical need to identify anoikis-related genes that distinctly impact the prognosis of PDAC.

To address this gap, we conducted comprehensive analyses leveraging RNA data and clinical features from public databases to establish risk signatures and molecular subtypes for PDAC patients. These signatures were based on expression levels of genes associated with anoikis, promising more robust prognostic predictions for PDAC patients. Additionally, we aimed to elucidate the interplay between anoikis-associated genes and the tumor microenvironment through functional studies.

Materials and Methods

Data Acquisition and Gene Selection

RNA sequencing data and clinical information for 150 PDAC patients, comprising 146 PDAC samples and four normal tissues adjacent to the tumor (NATs), were obtained from The Cancer Genome Atlas (TCGA) database (https://portal.gdc.cancer.gov/). A total of 338 genes associated with anoikis were retrieved from the GeneCards database (https://www.genecards.org/). Additionally, PDAC RNA sequencing data and related clinical data for a validation set of 234 patients were acquired from the International Cancer Genome Consortium (ICGC) through the Sangerbox web platform [19].

Identification of Differentially Expressed Genes (DEGs)

Differential expression analysis was conducted using Limma (linear models for microarray data), a method based on generalized linear models [20]. The R software limma (version 3.40.6, The Walter and Eliza Hall Institute of Medical Research, Melbourne, Australia) was employed to assess gene expression differences between the TCGA-PDAC and the NATs groups. A fold-change threshold of 1.5 was applied, and $p < 0.05$ considered statistically significant.

WGCNA and Correlation Analysis

A total of 54,469 gene expression profiles from 150 samples were subjected to weighted gene co-expression network analysis (WGCNA) to identify modular genes associated with the cancer phenotype. Initially, the Median Absolute Deviation (MAD) was computed for each gene using the gene expression profile. Subsequently, we filtered out the top 50% of genes with the smallest MAD and removed outlier genes and samples using the goodSamplesGenes method from the R software package WGCNA (version 1.72-5, University of California, Los Angeles, CA, USA), refining our dataset.

Next, we constructed a scale-free co-expression network using WGCNA, which enabled us to elucidate the relationship and functions of genes within the network. Additionally, Gene Ontology (GO) enrichment analysis and Kyoto Encyclopedia of Genes and Genomes (KEGG) pathway analysis were performed using the WebGestaltR package (version 0.4.6, Baylor College of Medicine, Houston, TX, USA) to assess the module genes. A significance threshold of $p < 0.05$ and false discovery rate (FDR) <0.1 was applied with a minimum gene set comprising at least 5 genes and a maximum gene set containing up to 5000 genes, which was considered statistically significant.

Acquisition of the Hub Anoikis-Related Genes (ARgs) and Gene Set Enrichment Analysis (GSEA)

To identify the hub ARgs, we conducted an intersection analysis among the DEGs, module genes, and anoikis-related genes. Subsequently, the samples were stratified into two groups based on the expression levels of the hub ARgs and used GSEA software (version 3.0, Broad Institute of Massachusetts Institute of Technology and Harvard, Cambridge, MA, USA) for analysis. Background gene sets were retrieved from the Molecular Signatures Database (http://www.gsea-msigdb.org/gsea/downloads.jsp), and GSEA was executed using the GSVA package (version 1.34.8, Hospital del Mar Medical Research Institute, Barcelona, Spain) to reveal the functional roles of each hub ARg. Significance was determined by a cutoff point of $|\text{normalized enrichment score (NES)}| > 1$ and false discovery rate (FDR) value <0.25 for GSEA analysis.

Development of a Prognostic Risk Signature Based on the Hub ARgs

Regression analysis was conducted using the R software package glmnet (version 4.1-2, Stanford University, San Francisco, CA, USA) and the least absolute shrinkage and selection operator/cyclooxygenase (LASSO-COX) method, which integrated survival time, survival

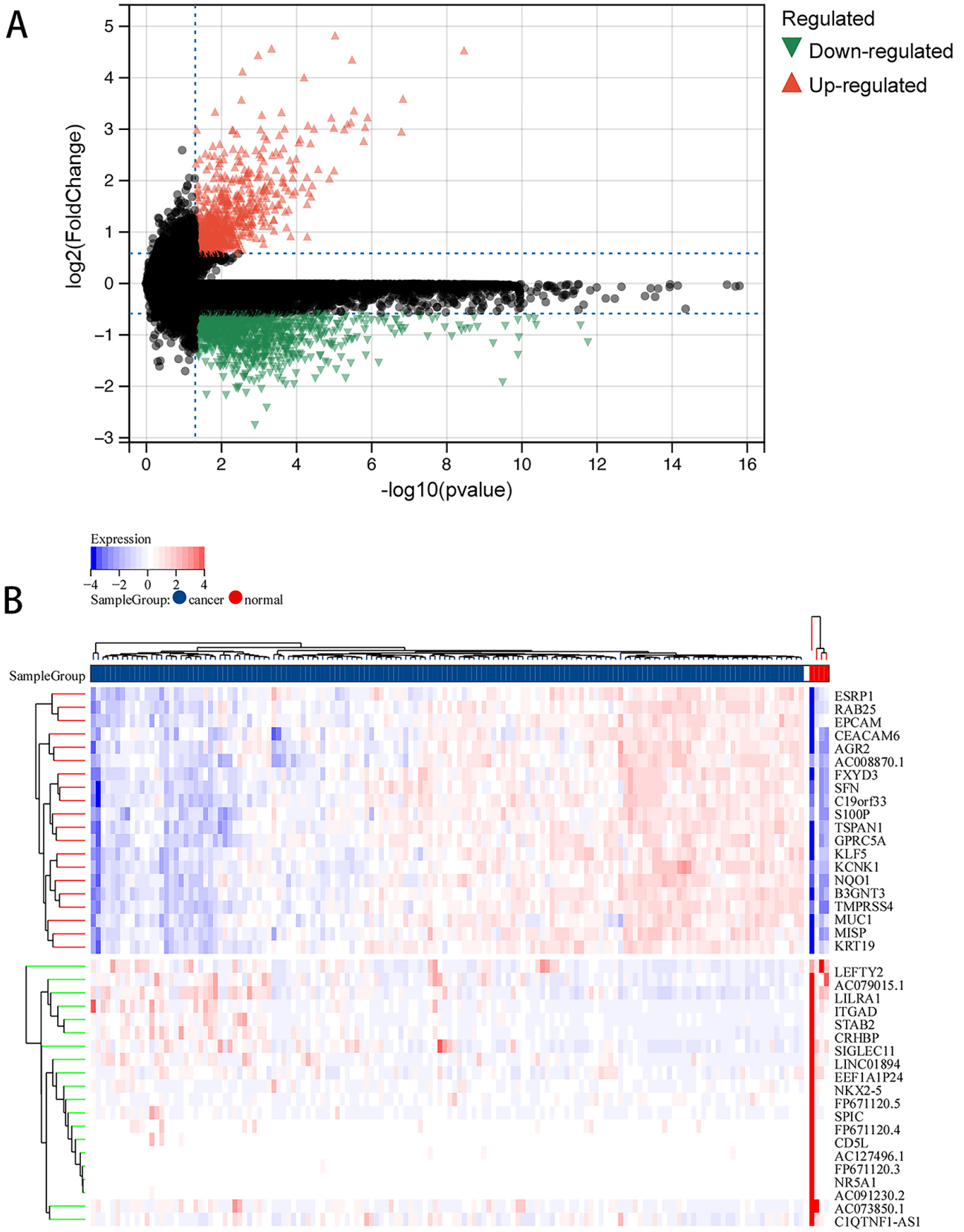

Fig. 1. Identification of differentially expressed genes. (A) The volcano plot illustrates the differentially expressed genes. (B) The heatmap displays the top 20 genes significantly overexpressed in pancreatic ductal adenocarcinoma (PDAC) or normal samples.

Journal of
BIOLOGICAL REGULATORS
and Homeostatic Agents

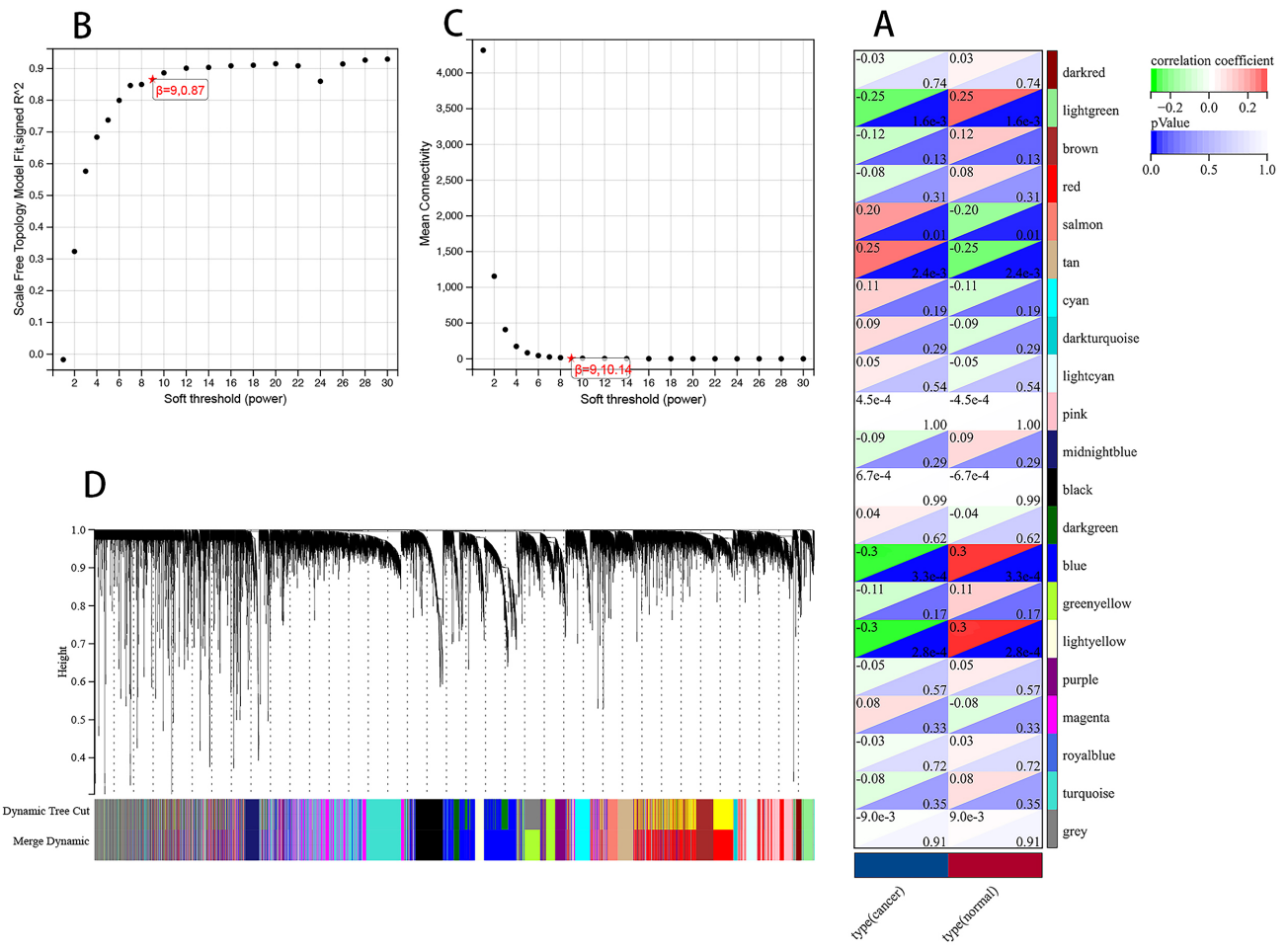

Fig. 2. Results of the weighted gene co-expression network analysis (WGCNA). (A) Correlation between different modules and clinical phenotypes (cancer or normal). (B) Average connectivity. (C) Mean connection values are associated with various soft threshold powers. (D) Gene cluster dendrogram. *$p < 0.05$.

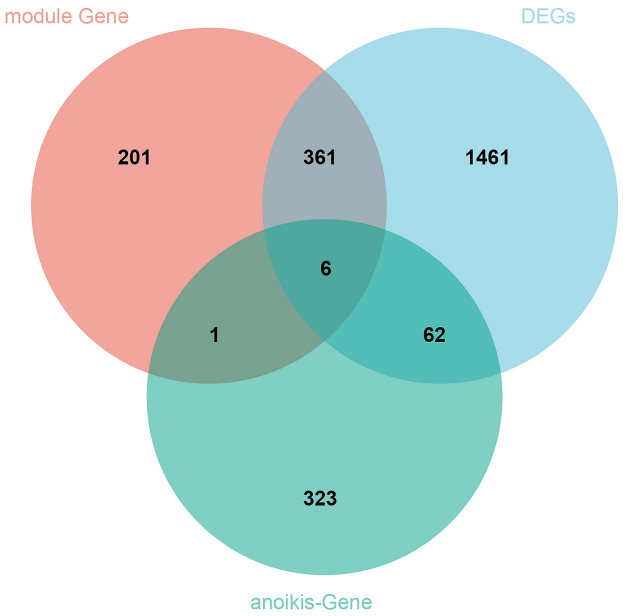

Fig. 3. Identification of hub anoikis-related genes. Six hub anoikis-related genes (ARgs) were identified by combining the differentially expressed genes (DEGs), WGCNA module genes, and anoikis-related genes.

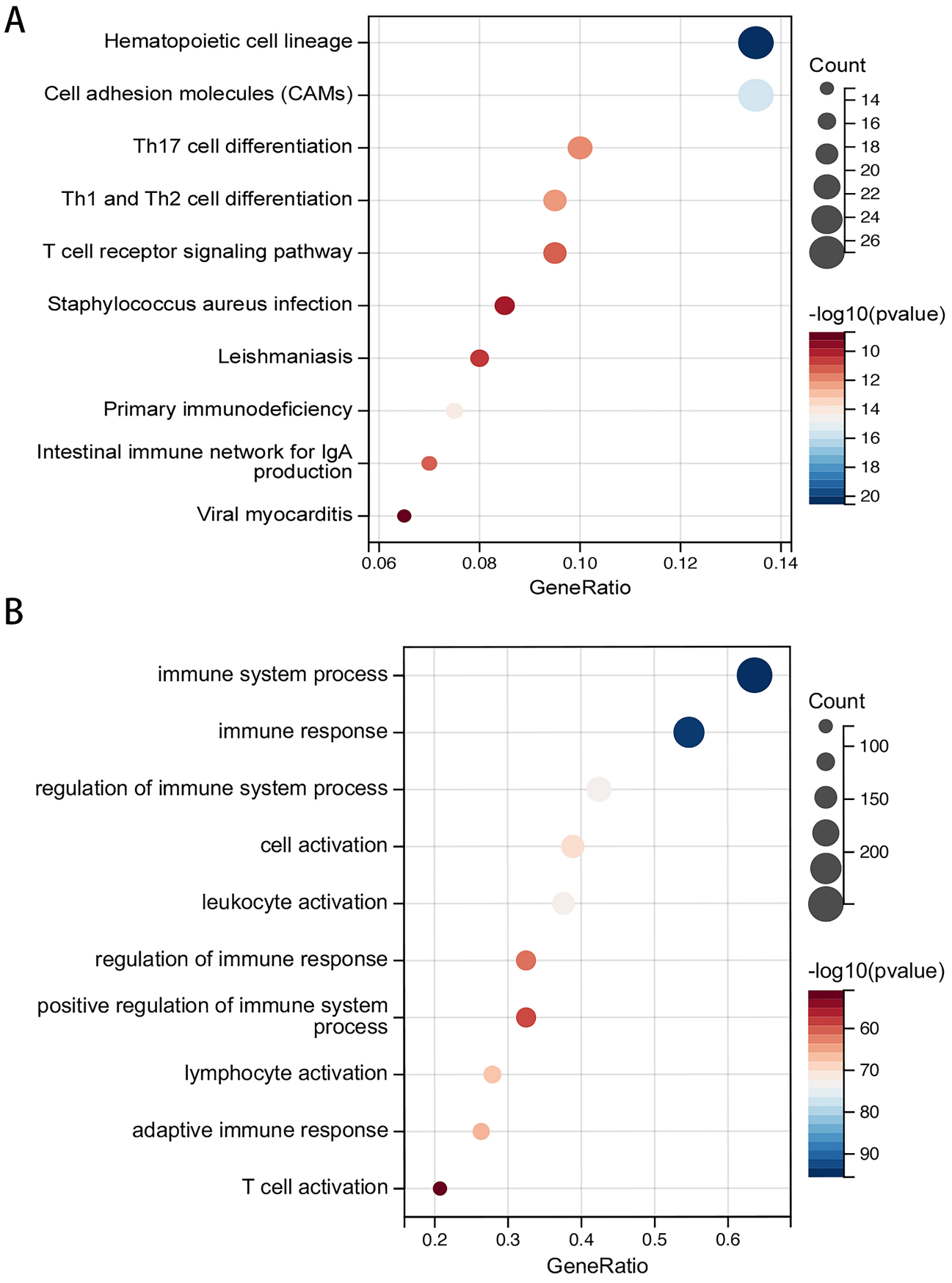

Fig. 4. Kyoto Encyclopedia of Genes and Genomes (KEGG) and Gene Ontology (GO) analysis. (A) KEGG analysis of the module genes. (B) GO analysis of the module genes.

Journal of
BIOLOGICAL REGULATORS
and Homeostatic Agents

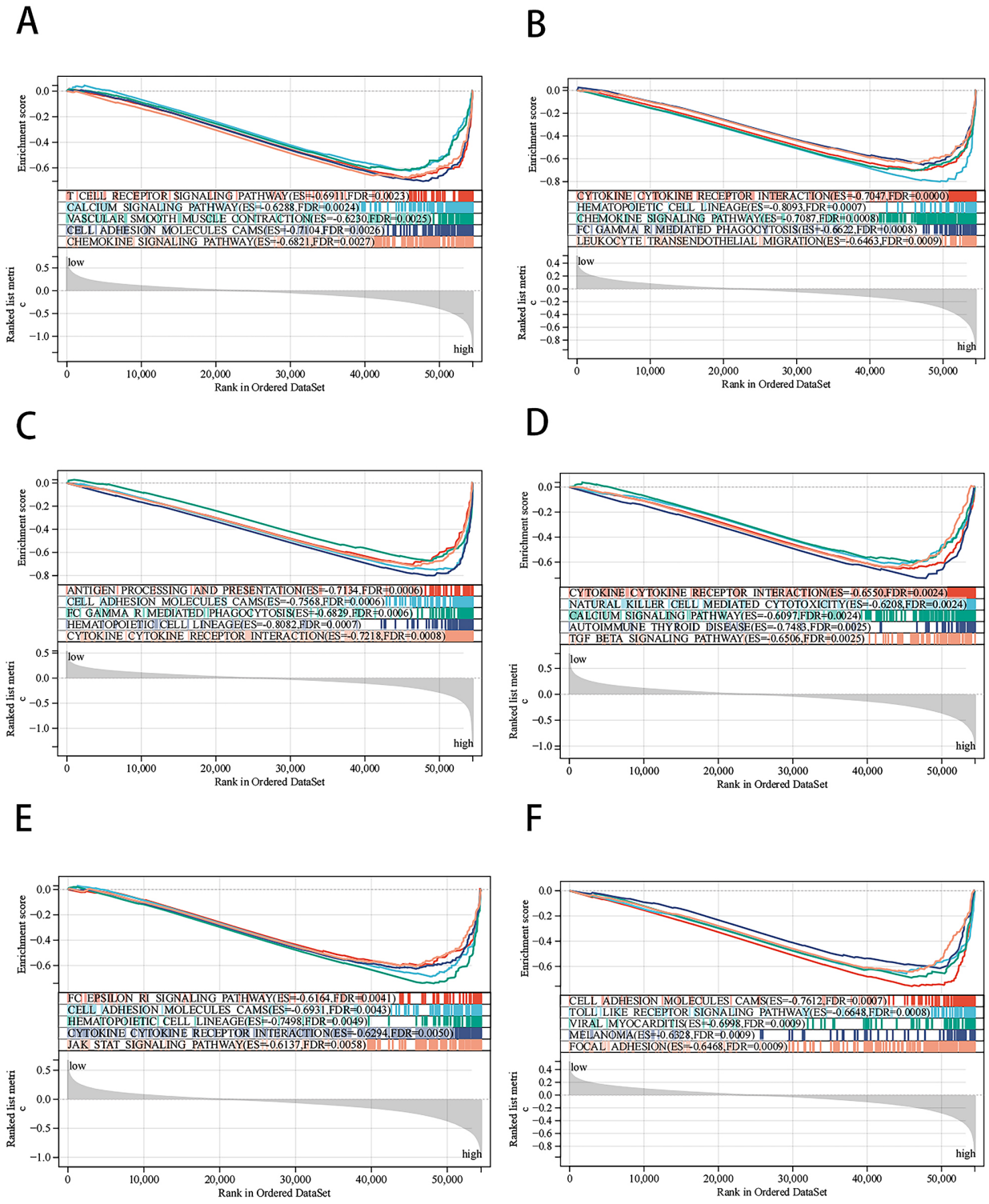

Fig. 5. Enriched pathways of hub ARgs were identified by GSEA. (A) BCL2, (B) CXCR4, (C) HAVCR2, (D) MYO5A, (E) SESN1, (F) SIRPA. GSEA, gene set enrichment analysis; BCL2, B-cell lymphoma-2; CXCR4, C-X-C motif chemokine receptor 4; HAVCR2, hepatitis A virus cellular receptor 2; MYO5A, myosin VA; SESN1, sestrin 1; SIRPA, signal-regulatory protein A.

state, and hub genes expression data. The optimal model was constructed through 10-fold cross-validation. Furthermore, the R package "maxstat" (Maximally chosen rank statistics with multiple *p*-value approximations: version 0.7-25, Ludwig-Maximilians-Universität München, München, Germany) was employed to determine an optimal RiskScore cut-off value. Subsequently, based on this threshold, the patient population was stratified into low-risk

and high-risk groups. To compare the prognosis between these groups, the survfit function from the survival package in R (version 3.5-7, University of Oslo, Oslo, Norway) was utilized, and significant differences in prognosis were defined using a log-rank test.

Receiver operating characteristic (ROC) curve analysis was conducted using the pROC package (version 1.17.0.1, University of Washington, Seattle, WA, USA) in R to calculate the area under the curve (AUC). Specifically, the ROC function of pROC was employed to gather patient follow-up duration and RiskScore data, and ROC analysis was performed at 365-day intervals.

Consensus Clustering Analysis and Construction of Molecular Subtypes Based on the Hub ARgs

Cluster analysis was performed using ConsensusClusterPlus (version 1.66, University of North Carolina at Chapel Hill, Chapel Hill, NC, USA) [21]. This analysis was performed iteratively with 80% of the samples, repeated 10 times, utilizing a Pearson correlation distance metric and agglomerative Pam clustering method. The optimal number of clusters was determined using the empirical cumulative distribution function plot.

Based on the expression values of the hub ARgs in each sample from the TCGA-PDAC dataset, the patients in TCGA dataset were analyzed by consistent cluster analysis and subtype was performed. The cumulative distribution function (CDF) curve demonstrated a steep ascent, enabling the optimal number of clusters to be determined. Subsequently, patients were stratified into distinct molecular subtypes based on the following criteria: the correlation between groups was the lowest and the intra-group correlation was the highest after clustering.

Tumor Immune Infiltration Characteristics Analysis between Subgroups

Utilizing our expression profile, we employed IOBR [22], an immune tumor biology computational tool, to calculate the CIBERSORT scores for 22 different types of immune invading cells in each sample [23]. Additionally, it allowed us to calculate the proportions of 22 immune cells in each of the two subgroups.

Tissue Samples

This study received approval from the Clinical Medical Research Ethics Committee of the Suzhou Ninth People's Hospital (approval number: 202232). Tumor and adjacent normal tissues were procured from Suzhou Ninth People's Hospital. All patients included in this study were not undergoing anticancer therapy and had provided informed consent prior to surgery. Tumor and precancerous tissues were obtained from a total of 10 postoperative patients under the supervision of an experienced pathology colleague.

Real-Time Polymerase Chain Reaction Assay

Total RNA extraction from each adipose tissue sample was performed using Trizol (Cat. # 740955.50, Takara, Shiga, Japan). Subsequently, the concentration and purity of the extracted RNA were assessed using a NanoDrop Spectrophotometer (NanoDrop Technologies Inc., Wilmington, DE, USA). cDNA was synthesized from mRNA using a cDNA synthesis kit (Cat. # 639506, Takara, Shiga, Japan).

Quantitative real-time PCR was conducted using an SYBR Green Premix Pro Taq HS qPCR kit (Cat. # 740703, Takara, Shiga, Japan). Relative gene expression levels were determined and normalized to *GAPDH* using the $2^{-\Delta\Delta Ct}$ method. All reactions were conducted in triplicate using an ABI 7300HT instrument (Applied Biosystems, ThermoFisher scientific, Waltham, MA, USA). Statistical analyses were conducted using GraphPad Prism 8.0 (GraphPad Software, Inc., San Diego, CA, USA), employing the 2-tailed Student *t*-test. Differences in transcriptome levels were assessed using Spearman's R. The list of primer pairs utilized in the assay is shown in **Supplementary Table 1**.

Results

Identification of Hub ARgs

Initially, we identified 1890 differentially expressed genes from the TCGA-PDAC dataset, with 683 genes showing up-regulation and 1207 genes displaying down-regulation. Fig. 1A depicts these genes, while Fig. 1B shows the top 20 differentially expressed genes.

Using the TCGA-PDAC expression profile, we constructed a weighted gene co-expression network following the removal of anomalous samples and gene filtering. To evaluate their correlation with tumor phenotypes, we generated a heat map depicting 21 co-expression modules represented by various colors (Fig. 2A,D). The average connectivity was calculated as 10.14, with a scale-free fit index of 0.87 (Fig. 2B) and a soft threshold of 9 (Fig. 2C). Notably, the blue and light-yellow modules exhibited statistically significant associations with cancer (blue modules: $r = –0.3$, $p = 3.3 \times 10^{-4}$; light-yellow module: $r = –0.3$, $p = 2.8 \times 10^{-4}$). Based on these results, a total of 569 genes from these two modules were designated as module genes. The hub ARgs were subsequently selected through the intersection of DEGs, anoikis-related genes, and module genes (Fig. 3).

Moreover, we conducted a KEGG enrichment analysis of the module genes. Our findings revealed significant enrichment in Th17, Th1, and Th2 cell differentiation, T Cell Receptor Signaling Pathway, Hematopoietic Cell Lineage, and Cell Adhesion Molecules (CAMs) (Fig. 4A). Subsequently, we performed GO analysis on the module genes. The findings indicated a strong association between immune system processes and immune responses, which exhibited the highest statistical significance (Fig. 4B). No-

Journal of
BIOLOGICAL REGULATORS
and Homeostatic Agents

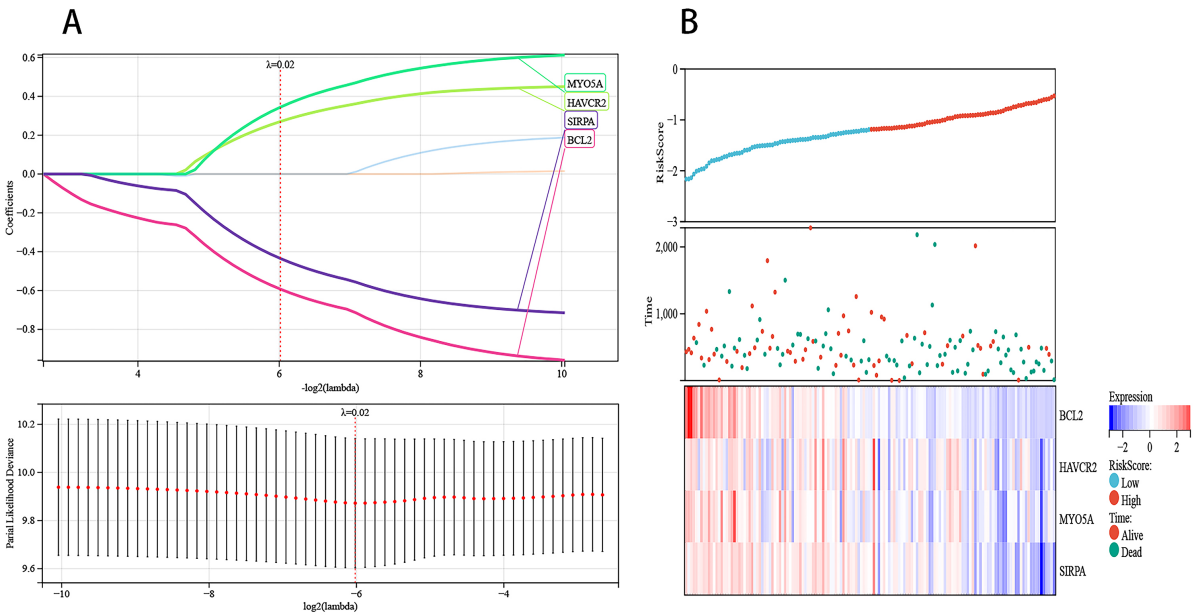

Fig. 6. Construction of risk signature in The Cancer Genome Atlas (TCGA) cohort. (A) Least absolute shrinkage and selection operator (LASSO) regression of the 6 overall survival (OS)-related hub ARgs. (B) RiskScore distribution of a pancreatic ductal adenocarcinoma (PDAC) patient based on ARgs. The association between the OS and the RiskScore for PDAC patients according to the signature is shown in the scatter plots.

tably, functions such as regulation of the immune system process, immune system process, and immune response were prominently enriched.

GSEA and Enrichment Analysis

Using GSEA, we evaluated the signaling pathways associated with hub ARgs. Our findings indicate that these genes are associated with various pathways, including calcium signaling pathway, Cell Adhesion Molecules (CAMs), cytokine-cytokine receptor interaction, chemokine signaling pathway, and hematopoietic cell lineage (Fig. 5).

Development of a Prognostic Gene Signature

LASSO-COX regression was employed, with the lambda value set to 0.0154387394424353, yielding the following model formula with four hub ARgs (Fig. 6):

$$RiskScore = 0.5929 \times BCL2 + 0.2705 \times HAVCR2 + 0.3444 \times MYO5A - 0.4350 \times SIRPA$$

The overall survival (OS) analysis revealed a shorter survival time for high-risk patients than low-risk patients, as illustrated by the Kaplan-Meier curve and distribution map ($p = 1.6 \times 10^{-4}$). Additionally, the area under the curve (AUC) for 1-year survival time was calculated to be 0.71 (Fig. 7).

Consensus Clustering Analysis and Classification of Molecular Subtypes Based on Hub ARgs

To further explore the characteristics of ARgs in PDAC patients, we also selected six Hub ARgs for clustering. Our findings indicated that K = 2 yielded the highest intra-cluster correlation (Fig. 8A), suggesting effective segregation of patients into two groups based on these six ARgs. Fig. 8B,C show the differences in the area under the cumulative distribution function (CDF) curve when varying the K for uniform clustering. However, no statistically significant prognostic differences were observed between the two cluster groupings, as evidenced by Kaplan-Meier survival curves based on these two clusters (HR = 0.94, 95% CI = 0.60–1.46, $p = 0.77$, Fig. 8D). Consequently, we further examined the composition ratio of patients in the two risk signature subgroups and the cluster subgroup through the Sankey chart (Fig. 9). Notably, high-risk patients and those in the C1 group exhibited significant differences compared to those in the low-risk and the C2 groups.

Subsequently, we compared the survival rates of the two subgroups following the regrouping by Sankey analysis. We observed a worse prognosis among patients in the high-risk+C1 group (HR = 0.43, 95% CI = 0.21–0.87, $p = 0.02$, Fig. 10A). Moreover, the AUC values for 1, 2, and 3-year survival periods were determined to be 0.73, 0.74, and 0.71, respectively (Fig. 10B). Our findings suggest that combining RiskScore and cluster analysis represents a novel classification method to further screen and classify patients.

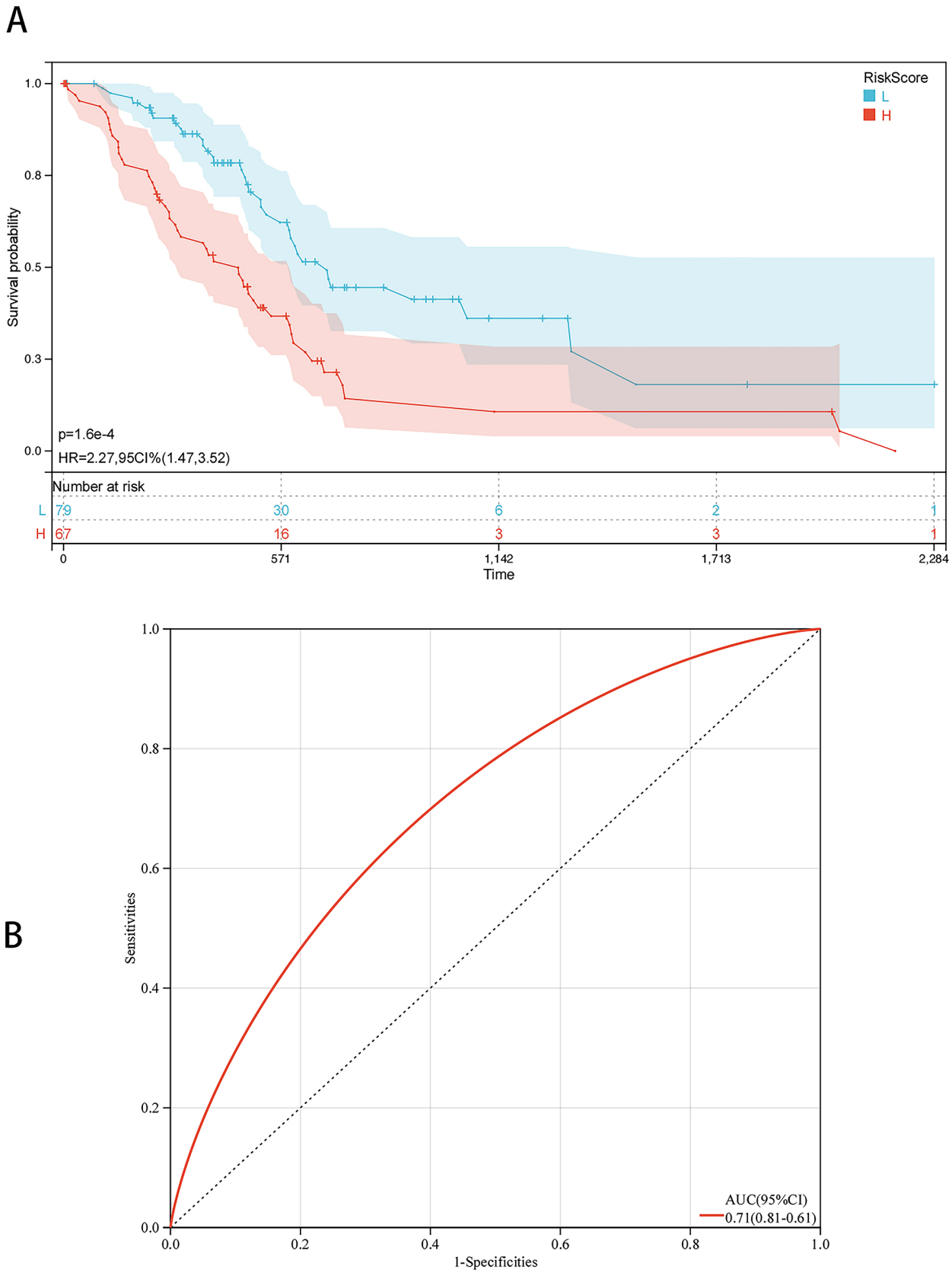

Fig. 7. Evaluation of the risk signature. (A) Kaplan-Meier survival analysis curves of the high- and low-risk groups in the TCGA database separated by the signature. (B) Time-dependent receiver operating characteristic (ROC) curve for the patients in the TCGA-PDAC at 1-year follow-up.

Journal of
BIOLOGICAL REGULATORS
and Homeostatic Agents

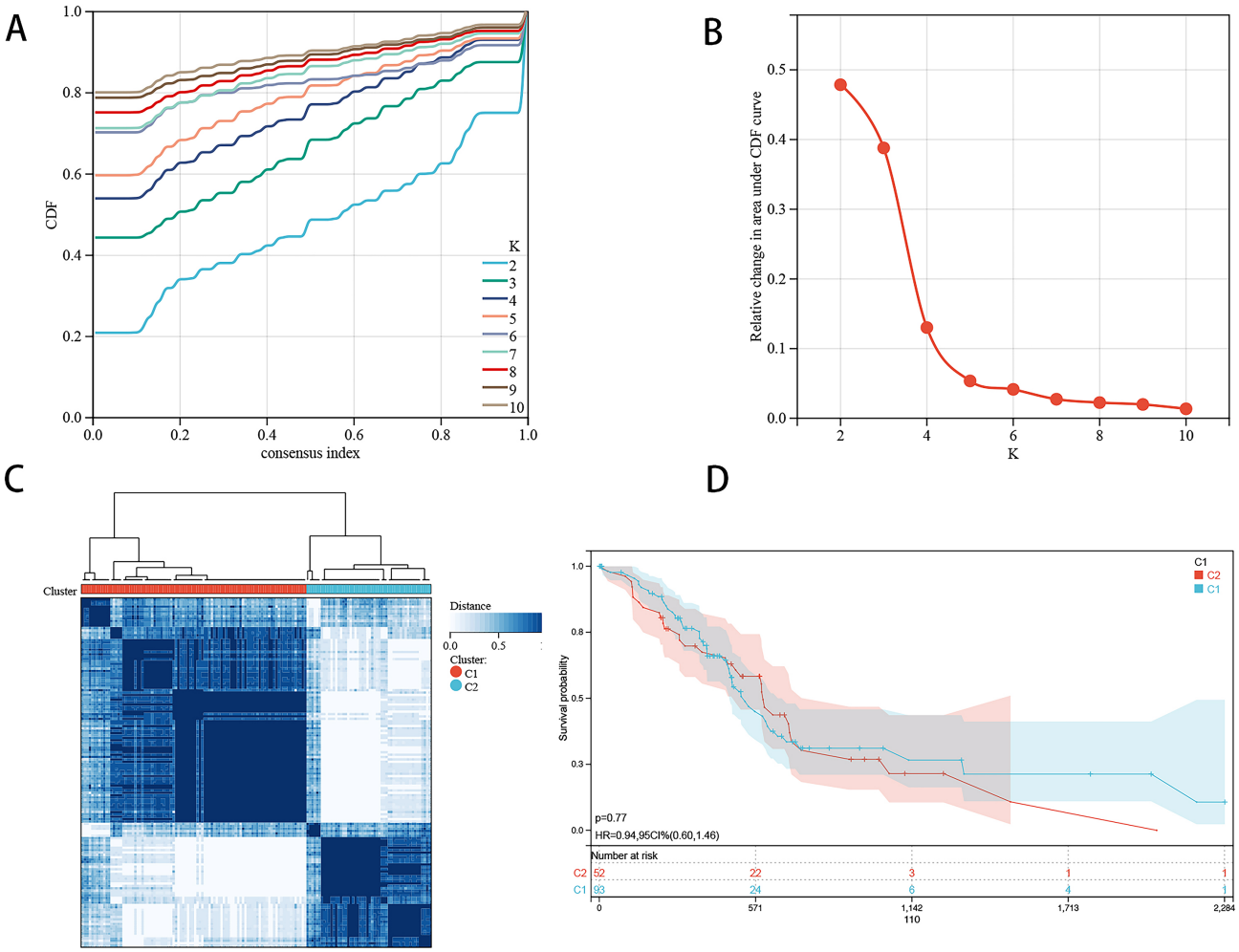

Fig. 8. Consensus clustering analysis based on hub ARgs in TCGA-PDAC. (A) Distribution of the cumulative distribution function (CDF) curve for consensus clustering. (B) Relative shift in the area under the curve (AUC) of the CDF curve at K = 2–10. (C) Examination of unsupervised clusters based on hub ARgs. (D) Kaplan-Meier plot in OS contrasting clusters 1 and 2 in OS.

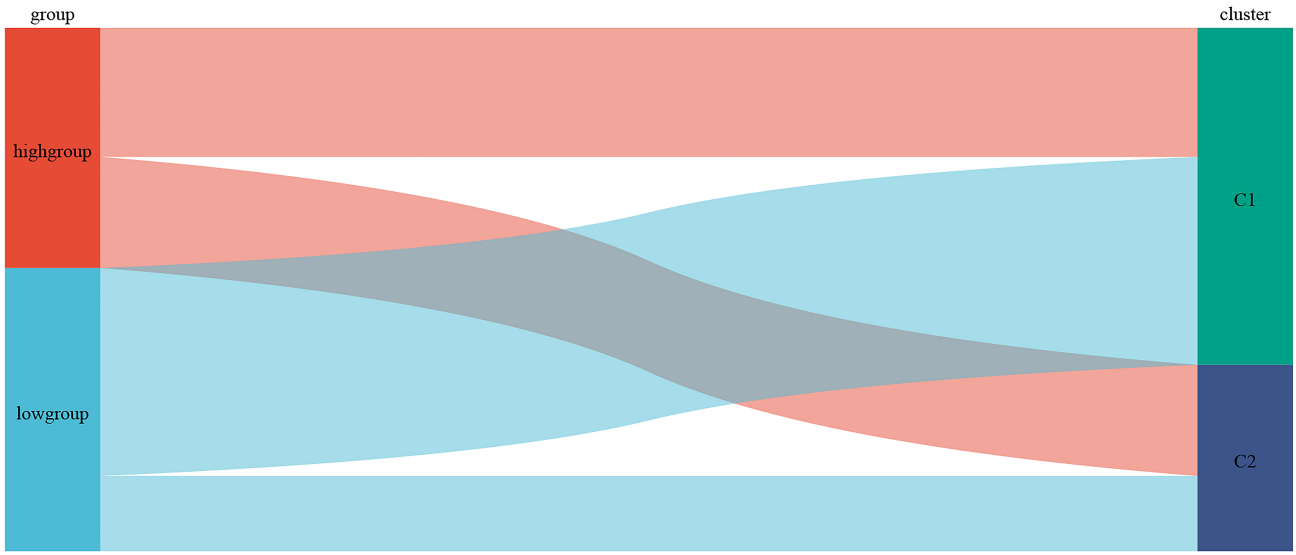

Fig. 9. Sankey diagram of the two subgroups (C1 and C2 subjected to gene clustering) and two risk groups.

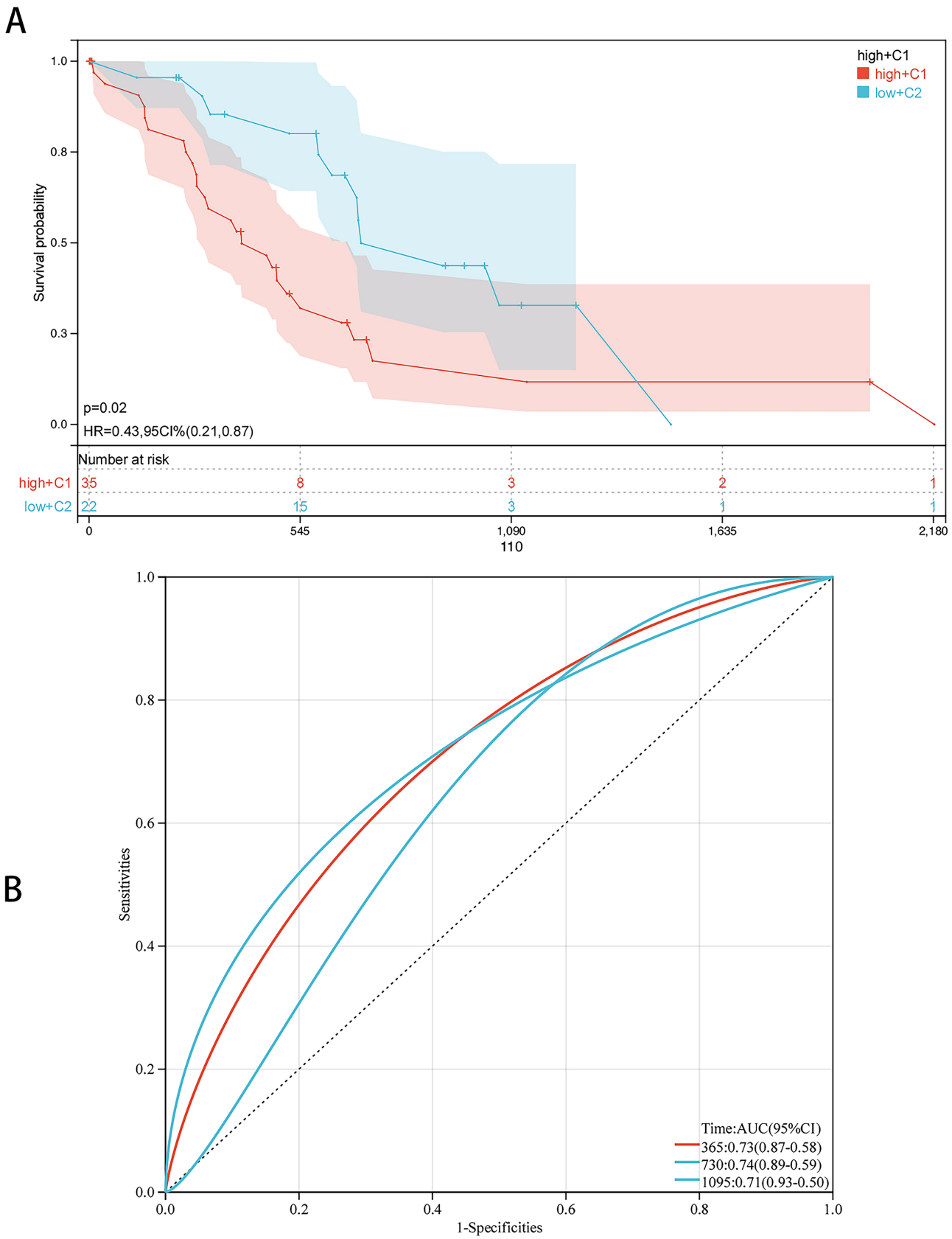

Fig. 10. Assessments of the new classifications. (A) Kaplan-Meier survival analysis curves are separated by the new classification into the high-risk+C1 and low-risk+C2 groups. (B) Time-dependent ROC curves for the TCGA-PDAC patients at 1, 2, and 3 years of follow-up.

Journal of
BIOLOGICAL REGULATORS
and Homeostatic Agents

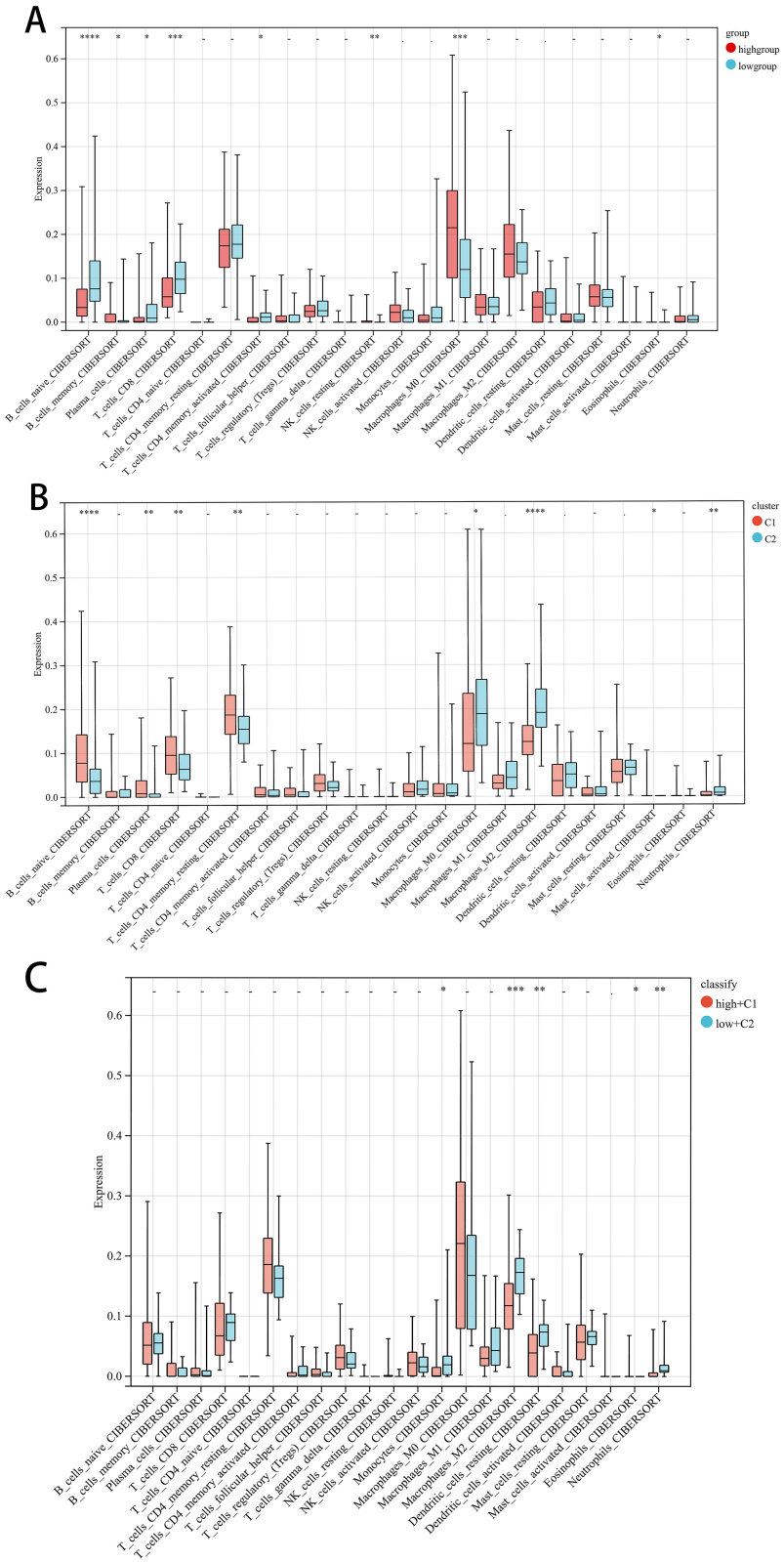

Fig. 11. Correlation between different subgroups and immune cell infiltration levels in PDAC patients. (A) The box plots show significantly different immune cell levels between the high-risk and low-risk subgroups. (B) The box plots illustrate significantly different immune cell levels between the C1 and C2 subgroups. (C) The box plots demonstrate the varying immune cell infiltration levels between the high+C1 group and the low+C2 group after adopting the new classification method. *$p < 0.05$, **$p < 0.01$, ***$p < 0.001$, ****$p < 0.0001$.

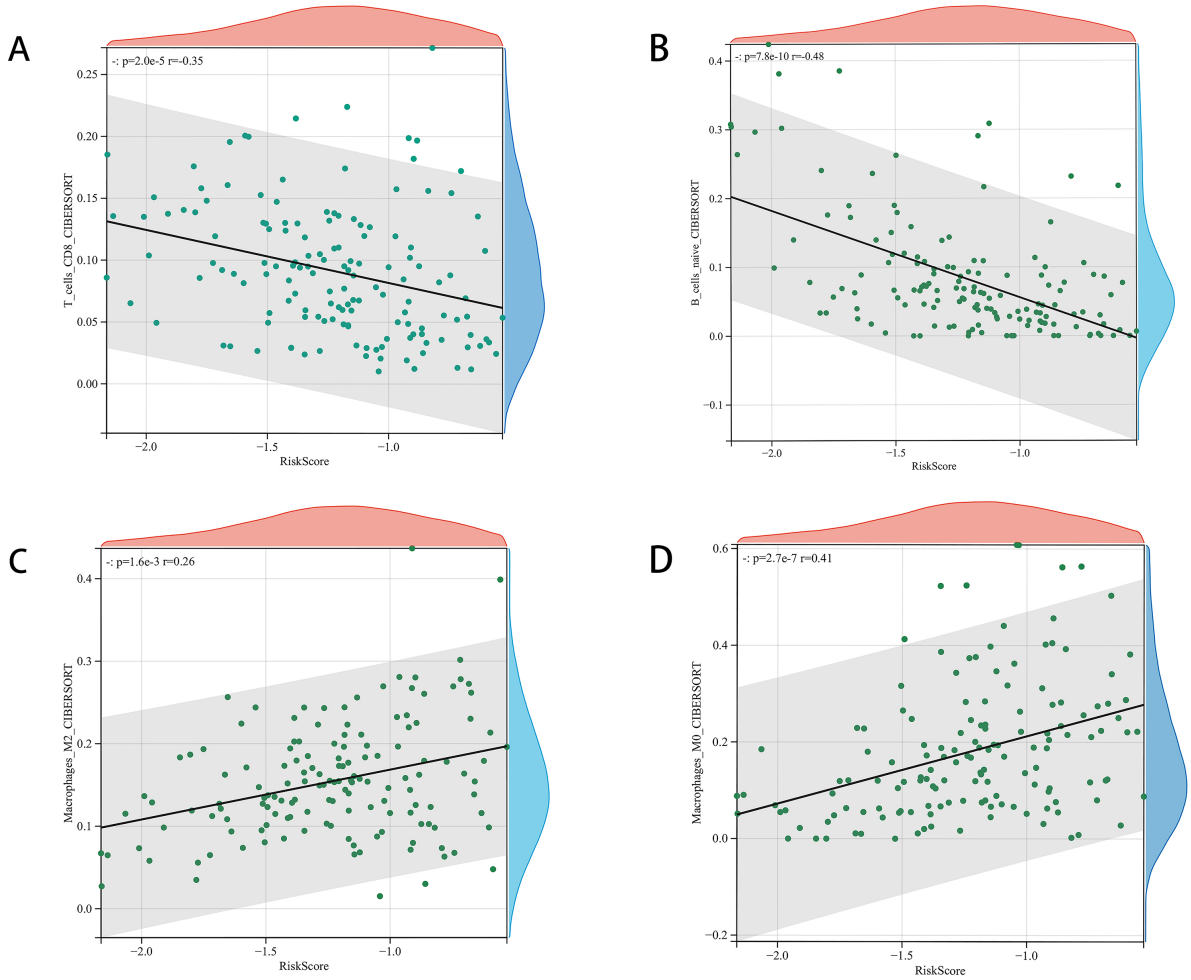

Fig. 12. Correlation of the risk signature with the immune cells, including (A) T cells CD8, (B) B cells naïve, (C) Macrophages M2, and (D) Macrophages M0.

Subtype-Based Analysis of Immunological Features

We employed the "CIBERSORT" algorithm to determine the differences in immune cell infiltration between the C1 and C2 clusters, representing high-risk and low-risk subgroups. Notably, significant variations were observed in B cells naive, T cells CD8, plasma cells, and macrophage M0. In the low-risk group, the infiltration level of macrophages M0 was lower than in the high-risk group, with the C1 cluster exhibiting a lower infiltration level compared to the C2 cluster. Conversely, in the high-risk group, the infiltration level of B cells naive, T cells CD8, and plasma cells was also lower compared to the low-risk group, and the C2 cluster exhibited a lower infiltration level compared to the C1 cluster.

Similarly, following the implementation of the new classification approach, we compared immune cell levels in the high+C1 and low+C2 groups. Our analysis revealed that the levels of M2 macrophages, resting dendritic cells, and neutrophils were lower in the high+C1 group, indicating a worse prognosis in comparison to the low+C2 group (Fig. 11).

Overall, we explored the correlation between immune cells and risk signatures. Our findings revealed that an increase in the RiskScore was associated with lower levels of CD8 T cells and naive B cells but higher levels of macrophages (M0 and M2) (Fig. 12).

Validation of the Novel Categorization and the Anoikis-Related Prognostic Risk Signature

Using ICGC datasets, we validated the performance of the anoikis-related predictive risk signature. Our analysis revealed that patients with high-RiskScores exhibited lower survival rates and higher mortality (HR = 1.37, 95% CI = 1.02–1.85, $p = 0.04$, Fig. 13A). Additionally, the AUC for the one-year survival time of prognostic signature in the ICGC dataset was 0.66 (Fig. 13B). Subsequently, through the expression of six hub ARgs, patients were categorized into C1 and C2 subclusters via cluster analysis (Fig. 14). With the application of this novel classification method, the Kaplan-Meier curve results for high-risk C1 subgroup patients and low-risk C2 subgroup patients mirrored those in the TCGA dataset. Furthermore, a more significant statis-

Journal of
BIOLOGICAL REGULATORS
and Homeostatic Agents

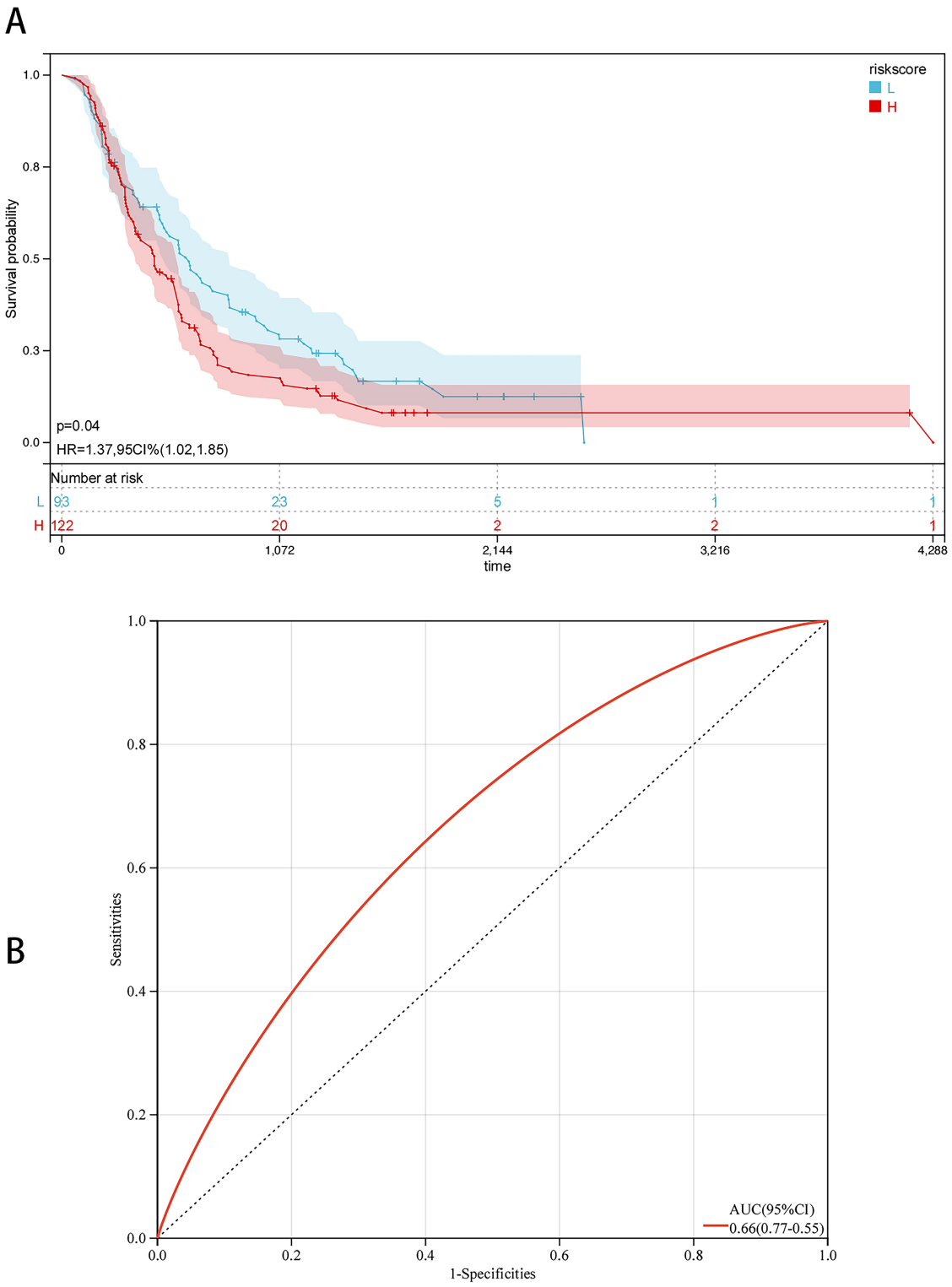

Fig. 13. Assessments of the risk signature in the International Cancer Genome Consortium (ICGC) database. (A) Kaplan-Meier survival analysis curves of the high- and low-risk groups in the ICGC database, separated by the signature. (B) Time-dependent ROC curves for the patient in ICGC-PDAC at 1 year of follow-up.

tical difference was observed (HR = 0.49, 95% CI = 0.32–0.75, $p = 8.9 \times 10^{-4}$, Fig. 15A), with AUC values of 0.66, 0.64, and 0.68 at 1, 2, and 3 years, respectively (Fig. 15B). These results underscored the high predictability of overall survival conferred by the newly developed classification method and the risk prediction signature based on genes related to anoikis.

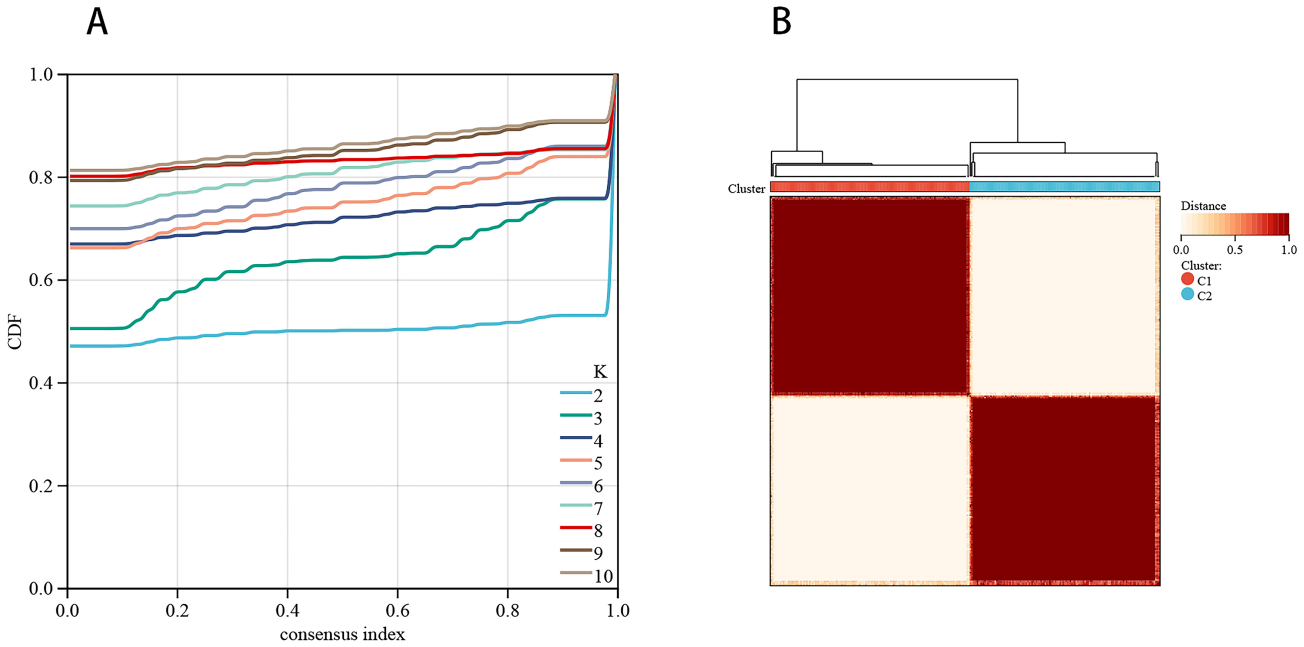

Fig. 14. Consensus clustering based on hub ARgs in ICGC-PDAC. (A) Relative shift in the area under the curve of the CDF curve at K = 2–10. (B) Examination of unsupervised clusters based on hub ARgs.

Verification of Hub Genes in PDAC Tissues through PCR Assay

PCR was conducted to further confirm the expressions of hub genes in clinical samples. The results revealed significant down-regulation of B-cell lymphoma-2 (*BCL2*), *CACR4*, and hepatitis A virus cellular receptor 2 (*HAVCR2*) expressions in pancreatic ductal adenocarcinoma tissues compared to the adjacent tissues (**Supplementary Fig. 1**). The expressions of myosin VA (*MYO5A*), *SESNE1*, and signal-regulatory protein A (*SIRPA*) were not statistically significant but consistent with the results of bioinformatics analysis.

Discussion

By 2030, the absolute death rate of pancreatic cancer is projected to rank second only to lung cancer, making it the second-leading cause of cancer-related deaths worldwide [24]. The challenge of early diagnosis and poor prognosis of patients underscores the urgent need for effective interventions. Epidemiological data from 2022 revealed a median survival time of less than 20 months for pancreatic cancer patients post-surgery [3]. Despite comprehensive systemic therapies, including surgery, chemotherapy, radiotherapy, targeted therapy, and immunotherapy [25], effectively extending patient survival remains elusive. Therefore, elucidating accurate biomarkers to detect the associated molecular subtypes of PADC and predict patient outcomes is paramount for guiding precise and personalized treatment strategies.

The extracellular matrix (ECM) is a pivotal non-cellular component that regulates various cell behaviors and mediates cell communication. Its role in influencing cell migration, proliferation, tumor metastasis, and treatment resistance mechanisms in pancreatic cancer is increasingly recognized [26]. Anoikis, coined in 1994, has been predominantly studied for its ability to suppress abnormal cell proliferation or detachment from the ECM [27], playing a pivotal role in tumor progression [28–30]. However, research on the collective impact of ARgs in PDAC patients has been limited.

In this study, the differential expression of ARgs in PDAC laid the foundation for developing a robust and reliable prognostic signature. We identified two distinct molecular subtypes and examined the interactions between ARgs and the clinical tumor immune microenvironment. By integrating these findings, we have established a novel classification system to facilitate more precise and personalized PDAC treatment approaches for PDAC patients.

In this study, we initially explored a total of 68 differentially expressed ARgs in the TCGA-PDAC dataset. Subsequently, we employed the WGCNA method to identify 7 modules of ARgs associated with tumor phenotype, from which 6 hub ARgs (*BCL2*, C-X-C motif chemokine receptor 4 (*CXCR4*), *HAVCR2*, *MYO5A*, sestrin 1 (*SESN1*), *SIRPA*) were identified through the intersection. Next, employing the LASSO-COX approach, we constructed a risk signature comprising four hub ARgs to predict the prognosis of PDAC patients, categorizing them as low-risk or high-risk groups. Notably, significant variations in prognosis and immune infiltration were observed between these

Journal of
BIOLOGICAL REGULATORS
and Homeostatic Agents

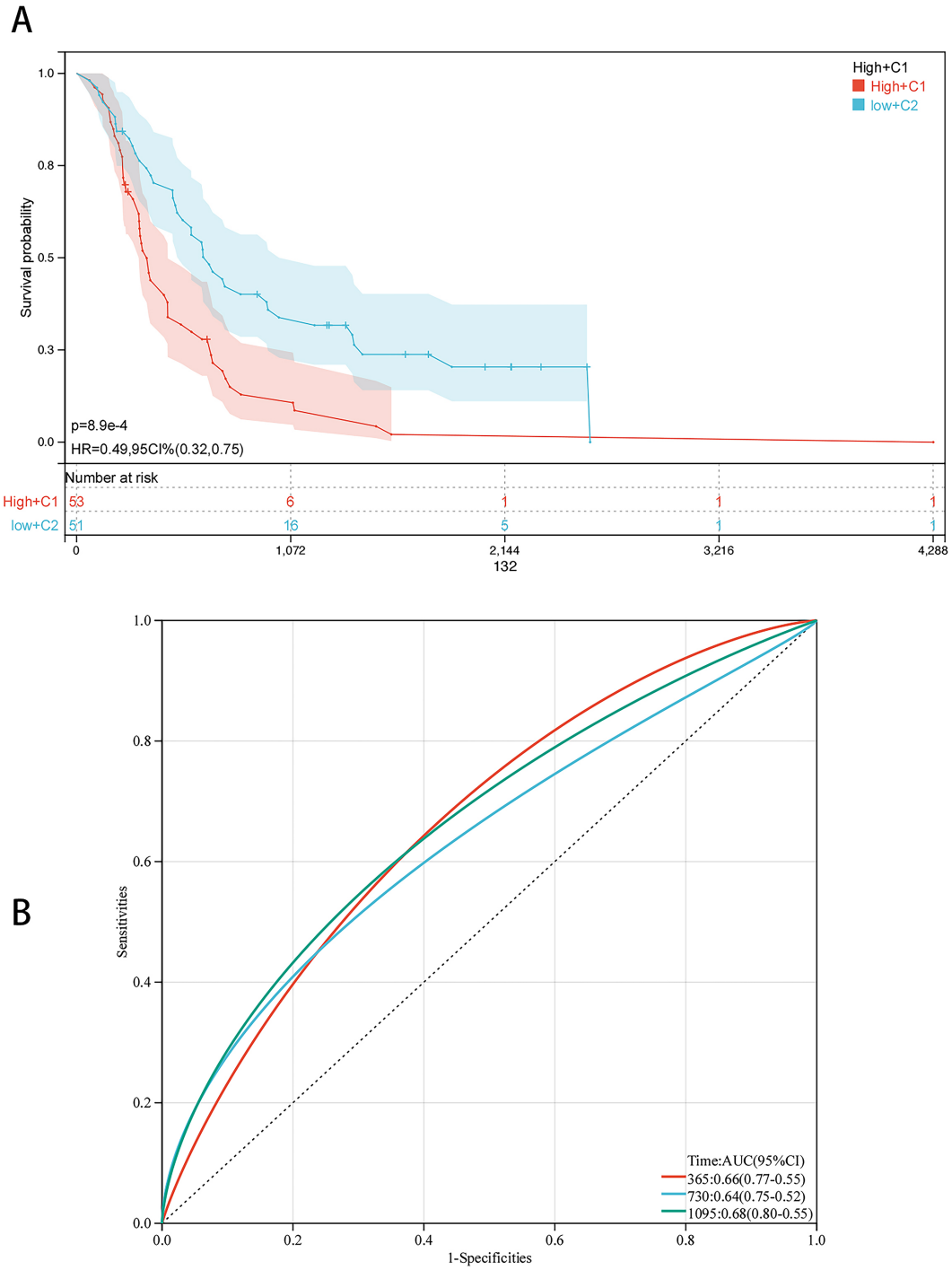

Fig. 15. Evaluation of the new classifications in the ICGC database. (A) Kaplan-Meier survival analysis curves, stratified by the new classification into the high-risk+C1 and low-risk+C2 categories. (B) Time-dependent ROC curves for the patients with ICGC-PDAC at 1, 2, and 3 years of follow-up.

two subgroups. Additionally, based on the expression patterns of the six hub ARgs, PDAC patients were separated into two molecular subgroups. However, Kaplan-Meier survival analysis did not reveal in overall survival (OS) differences between the two subtypes. Nevertheless, further analysis under the condition of immune infiltration unveiled distinct differences.

Furthermore, we observed an overlap between patients categorized by RiskScore and those classified by molecular subtypes, as depicted by the Sankey diagram. To enhance prognostic prediction, we combined the two approaches, thereby classifying patients into the High+C1 group and low+C2 group. Ultimately, we successfully externally validated the risk signature and the combined

screening model, confirming their significant predictive value. Our findings underscore the importance of developing robust molecular markers based on ARgs to enhance clinical management and reduce mortality rates among PDAC patients.

BCL2 is the pioneering anti-apoptotic gene discovered [31], exhibiting high expression levels in most pancreatic cancers [32]. The intricate interplay between pro-apoptotic (e.g., BAX) and anti-apoptotic (e.g., *BCL2*) members within the *BCL2* family determines cellular fate in response to apoptotic stimuli at the mitochondrial level [33,34]. *CXCR4*, a specific α-chemokine receptor for stromal cell-derived factor-1 (*SDF-1*) [35], plays a crucial role in PDAC. The *CXCR4-SDF-1* axis bridges the tumor and the stroma, contributing to tumor progression [36]. Recent findings have highlighted heightened *CXCR4* expression in CD8+ cells and macrophages in PDAC, suggesting its potential as a biomarker for assessing the efficiency of immune checkpoint inhibitors (ICI) [37]. Consequently, targeting *CXCR4*+ macrophage infiltration is crucial in PDAC immunotherapy [38].

HAVCR2, also referred to as T cell immunoglobulin 3 (Tim-3), is a marker of T cell failure. In PDAC, elevated expression of Tim-3 on T cells correlates with poorer prognosis [39,40]. Tim-3 promotes immunological invasion, evasion, and metastasis in pancreatic cancer [41]. Signal-regulatory protein A (*SIRPA*), a renowned transmembrane glycoprotein, produces protein byproducts that can enhance the response to immunotherapy in various malignancies.

The landscape of tumor therapy has shifted towards immunotherapy, with recent research highlighting the profound inhibition of pancreatic cancer in the immune environment [42]. Our results unveiled a significant correlation between hub ARgs and immune cell populations, prompting us to explore further their interaction within the immunological microenvironment. Accumulating evidence suggests the presence of CD8+ T cells in PDAC tumor tissue, and substantial infiltration is linked to markedly improved disease-free survival (DFS) and/or OS rates in PDAC patients [43,44]. Consistent with these findings, our study revealed a negative correlation between the risk signature and CD8 cells.

Additionally, 'hot' PDAC tumors are characterized by macrophage infiltration, which may lower the cytotoxic activity of CD8+ T cells [45]. Macrophages, often referred to as tumor-associated macrophages (TAMs), represent one of the most prevalent non-cancerous cell types in the tumor microenvironment (TME). Kurahara *et al*. [46,47] first reported the M2 polarization phenotype in human PDAC tissues, which correlates with enhanced lymph angiogenesis in lymph nodes and poor prognosis. Our findings corroborate the impact of macrophages on the overall survival (OS) of the patient, demonstrating a positive association between the risk signature and macrophages.

Further analysis of differences in immune cell infiltration between the two subgroups stratified by the risk signature revealed valuable insights. Despite higher M0 macrophage content in the high-risk group, native B cell, T cell CD8, and plasma cell contents were lower in this group with poorer prognosis. Similarly, although no prognostic differences were observed between the two subgroups identified by consistent cluster analysis, comparable immune cell infiltration patterns were evident. While group C2 exhibited high M0 Macrophage content compared to group C1, native B cell, T cell CD8, and plasma cell contents were lower in group C2 compared to group C1.

The convergence of immune infiltration patterns between C2 and high-risk groups post-reclassification underscores the rationale behind their classification overlap. Upon reclassification, we examined immune infiltration level variations between the high-risk+C1 and low-risk+C2 groups. We observed that some initial differences were eliminated following subgroup amalgamation, with notable differences in M2 macrophage, resting dendritic cells (DC), and neutrophils, and the group with poor prognosis had low expression.

DC is rare in the TME of PDAC, mainly located in the interstitial surrounding the tumor [48], and high levels of circulating DC in PDAC tissues are significantly correlated with improved OS [49,50]. DCs have emerged as the primary immune cells for developing anti-PDAC vaccines. Neutrophils have recently been identified as a key factor in promoting tumor metastasis, although their role in tumor progression remains contentious. In our findings, the expression of M0 macrophages was higher in the high-risk group, which also corresponds to a poor prognosis, while the high-risk+C1 group, another classification associated with poor prognosis, exhibited lower expression of M2 macrophages. The M2 phenotype of tumor-associated macrophages (TAMs) has an immunosuppressive effect. Previous study had indicated a predominance of M2-like TAMs in pancreatic cancer, with a corresponding decrease in overall survival as the number of M2 macrophages increases [51]. However, our findings are contrary to this finding. This might explain why there were no statistically significant differences in prognosis between the C1 and C2 groups.

This study identified genes related to anoikis and established a prognostic signature based on four hub ARgs to evaluate their value in estimating PDAC prognosis. Furthermore, we classified two molecular subtypes based on six hub ARgs through consistent cluster analysis. The combination of these molecular subtypes and the prognostic signature allowed for further stratification of patients, leading to improved prognosis assessment.

However, PDAC is a complicated and heterogeneous disease with various clinical characteristics. The genetic and epigenomic modifications contributing to diverse molecular, cellular, and clinical characteristics signif-

Journal of
BIOLOGICAL REGULATORS
and Homeostatic Agents

icantly increase inter- and intra-tumor heterogeneity, posing challenges in developing and managing PDAC. Extensive prospective clinical investigations are required to establish the function of anoikis in the onset and progression of diseases. This is also crucial for exploring its potential therapeutic benefits.

Conclusion

In conclusion, this comprehensive study examined the expression patterns and prognostic significance of ARgs in PDAC patients. Novel risk signatures were developed, and two molecular subtypes were classified for PDAC. Notably, the combination of risk signature with molecular subtypes accurately predicted the prognostic outcomes of PDAC patients. Additionally, we confirmed a close correlation between PDAC clinicopathological factors and the TME, and validated the prognostic signature and classification using external data from the ICGC. These findings offer new insights into the onset and progression of PDAC and antitumor targets, offering theoretical and practical support for the effective screening and follow-up treatment of PDAC patients.

Abbreviations

ARgs, anoikis-related genes; PDAC, pancreatic ductal adenocarcinoma; WGCNA, weighted gene co-expression network analysis; LASSO, least absolute shrinkage and selection operator; TCGA, The Cancer Genome Atlas; ICGC, International Cancer Genome Consortium; ECM, extracellular matrix; NATs, normal tissues adjacent to the tumor; DEGs, differentially expressed genes; Limma, linear models for microarray data; MAD, Median Absolute Deviation; GO, Gene Ontology; KEGG, Kyoto Encyclopedia of Genes and Genomes; GSEA, gene set enrichment analysis; ROC, receiver operating characteristic; AUC, area under the curve; CDF, cumulative distribution function; CAMs, Cell Adhesion Molecules; OS, overall survival; SDF-1, stromal cell-derived factor-1; ICI, immune checkpoint inhibitors; TME, tumor microenvironment; TAMs, tumor-associated macrophages; DC, dendritic cells.

Availability of Data and Materials

All data generated or analyzed during this study are included in this published article.

Author Contributions

Conceptualization: XL and MD; software: XL; writing-original draft preparation: MD and JL; writing-review and editing: XL and MD; visualization, prepared the figures: JL; data curation: JL; supervision: XL. All authors have been involved in revising it critically for important intellectual content. All authors gave final approval of the version to be published. All authors have participated sufficiently in the work to take public responsibility for appropriate portions of the content and agreed to be accountable for all aspects of the work in ensuring that questions related to its accuracy or integrity.

Ethics Approval and Consent to Participate

This study was approved by the Ethics Committee of the Suzhou Ninth People's Hospital (approval number: 202232). Patients/participants provided written informed consent to participate in this study.

Acknowledgment

Not applicable.

Funding

This research was supported by the Scientific Research Project Fund of Suzhou Ninth People's Hospital, Grant Number: KY2022-025-01.

Conflict of Interest

The authors declare no conflict of interest.

Supplementary Material

Supplementary material associated with this article can be found, in the online version, at https://doi.org/10.23812/j.biol.regul.homeost.agents.20243806.402.

References

[1] Sung H, Ferlay J, Siegel RL, Laversanne M, Soerjomataram I, Jemal A, *et al*. Global Cancer Statistics 2020: GLOBOCAN Estimates of Incidence and Mortality Worldwide for 36 Cancers in 185 Countries. CA: A Cancer Journal for Clinicians. 2021; 71: 209–249.

[2] Clinton SK, Giovannucci EL, Hursting SD. The World Cancer Research Fund/American Institute for Cancer Research Third Expert Report on Diet, Nutrition, Physical Activity, and Cancer: Impact and Future Directions. The Journal of Nutrition. 2020; 150: 663–671.

[3] Siegel RL, Miller KD, Fuchs HE, Jemal A. Cancer statistics, 2022. CA: A Cancer Journal for Clinicians. 2022; 72: 7–33.

[4] Torphy RJ, Fujiwara Y, Schulick RD. Pancreatic cancer treatment: better, but a long way to go. Surgery Today. 2020; 50: 1117–1125.

[5] Goggins M, Overbeek KA, Brand R, Syngal S, Del Chiaro M, Bartsch DK, *et al*. Management of patients with increased risk for familial pancreatic cancer: updated recommendations from the International Cancer of the Pancreas Screening (CAPS) Consortium. Gut. 2020; 69: 7–17.

[6] Huang C, Simeone DM, Luk L, Hecht EM, Khatri G, Kambadakone A, *et al*. Standardization of MRI Screening and Reporting in Individuals with Elevated Risk of Pancreatic Ductal Adenocarcinoma: Consensus Statement of the PRECEDE Consortium. AJR. American Journal of Roentgenology. 2022; 219: 903–914.

[7] Farrukh J, Balasubramaniam R, James A, Wadhwani SS, Albazaz R. Pancreatic adenocarcinoma: imaging techniques for diagnosis and management. British Journal of Hospital Medicine. 2022; 83: 1–12.
[8] Shi XH, Li X, Zhang H, He RZ, Zhao Y, Zhou M, *et al*. A Five-microRNA Signature for Survival Prognosis in Pancreatic Adenocarcinoma based on TCGA Data. Scientific Reports. 2018; 8: 7638.
[9] da Paixão VF, Sosa OJ, da Silva Pellegrina DV, Dazzani B, Corrêa TB, Risério Bertoldi E, *et al*. Annotation and functional characterization of long noncoding RNAs deregulated in pancreatic adenocarcinoma. Cellular Oncology (Dordrecht). 2022; 45: 479–504.
[10] Kandimalla R, Shimura T, Mallik S, Sonohara F, Tsai S, Evans DB, *et al*. Identification of Serum miRNA Signature and Establishment of a Nomogram for Risk Stratification in Patients with Pancreatic Ductal Adenocarcinoma. Annals of Surgery. 2022; 275: e229–e237.
[11] Kakavandi E, Shahbahrami R, Goudarzi H, Eslami G, Faghihloo E. Anoikis resistance and oncoviruses. Journal of Cellular Biochemistry. 2018; 119: 2484–2491.
[12] Adeshakin FO, Adeshakin AO, Afolabi LO, Yan D, Zhang G, Wan X. Mechanisms for Modulating Anoikis Resistance in Cancer and the Relevance of Metabolic Reprogramming. Frontiers in Oncology. 2021; 11: 626577.
[13] Fanfone D, Wu Z, Mammi J, Berthenet K, Neves D, Weber K, *et al*. Confined migration promotes cancer metastasis through resistance to anoikis and increased invasiveness. eLife. 2022; 11: e73150.
[14] Raeisi M, Zehtabi M, Velaei K, Fayyazpour P, Aghaei N, Mehdizadeh A. Anoikis in cancer: The role of lipid signaling. Cell Biology International. 2022; 46: 1717–1728.
[15] Yang X, Zhu Z, Liang T, Lei X. Comprehensive analysis of anoikis-related genes in prognosis and immune infiltration of gastric cancer based on bulk and single-cell RNA sequencing data. Journal of Cancer Research and Clinical Oncology. 2023; 149: 13163–13173.
[16] Zhang D, Wang Y, Zhou H, Han X, Hou L, Lv Z, *et al*. The study of an anoikis-related signature to predict glioma prognosis and immune infiltration. Journal of Cancer Research and Clinical Oncology. 2023; 149: 12659–12676.
[17] He Z, Gu Y, Yang H, Fu Q, Zhao M, Xie Y, *et al*. Identification and verification of a novel anoikis-related gene signature with prognostic significance in clear cell renal cell carcinoma. Journal of Cancer Research and Clinical Oncology. 2023; 149: 11661–11678.
[18] Xiao Y, Zhou H, Chen Y, Liu L, Wu Q, Li H, *et al*. A novel anoikis-related gene prognostic signature and its correlation with the immune microenvironment in colorectal cancer. Frontiers in Genetics. 2023; 14: 1186862.
[19] Shen W, Song Z, Zhong X, Huang M, Shen D, Gao P, *et al*. Sangerbox: a comprehensive, interaction-friendly clinical bioinformatics analysis platform. iMeta. 2022; 1: e36.
[20] Ritchie ME, Phipson B, Wu D, Hu Y, Law CW, Shi W, *et al*. limma powers differential expression analyses for RNA-sequencing and microarray studies. Nucleic Acids Research. 2015; 43: e47.
[21] Wilkerson MD, Hayes DN. ConsensusClusterPlus: a class discovery tool with confidence assessments and item tracking. Bioinformatics (Oxford, England). 2010; 26: 1572–1573.
[22] Zeng D, Ye Z, Shen R, Yu G, Wu J, Xiong Y, *et al*. IOBR: Multi-Omics Immuno-Oncology Biological Research to Decode Tumor Microenvironment and Signatures. Frontiers in Immunology. 2021; 12: 687975.
[23] Newman AM, Liu CL, Green MR, Gentles AJ, Feng W, Xu Y, *et al*. Robust enumeration of cell subsets from tissue expression profiles. Nature Methods. 2015; 12: 453–457.
[24] Rahib L, Smith BD, Aizenberg R, Rosenzweig AB, Fleshman JM, Matrisian LM. Projecting cancer incidence and deaths to 2030: the unexpected burden of thyroid, liver, and pancreas cancers in the United States. Cancer Research. 2014; 74: 2913–2921.
[25] Barcellini A, Peloso A, Pugliese L, Vitolo V, Cobianchi L. Locally Advanced Pancreatic Ductal Adenocarcinoma: Challenges and Progress. OncoTargets and Therapy. 2020; 13: 12705–12720.
[26] Naba A, Clauser KR, Ding H, Whittaker CA, Carr SA, Hynes RO. The extracellular matrix: Tools and insights for the "omics" era. Matrix Biology: Journal of the International Society for Matrix Biology. 2016; 49: 10–24.
[27] Giancotti FG, Tarone G. Positional control of cell fate through joint integrin/receptor protein kinase signaling. Annual Review of Cell and Developmental Biology. 2003; 19: 173–206.
[28] Paoli P, Giannoni E, Chiarugi P. Anoikis molecular pathways and its role in cancer progression. Biochimica et Biophysica Acta. 2013; 1833: 3481–3498.
[29] Tan K, Goldstein D, Crowe P, Yang JL. Uncovering a key to the process of metastasis in human cancers: a review of critical regulators of anoikis. Journal of Cancer Research and Clinical Oncology. 2013; 139: 1795–1805.
[30] Yang J, Zheng Z, Yan X, Li X, Liu Z, Ma Z. Integration of autophagy and anoikis resistance in solid tumors. Anatomical Record (Hoboken, N.J.: 2007). 2013; 296: 1501–1508.
[31] Korsmeyer SJ. Bcl-2 initiates a new category of oncogenes: regulators of cell death. Blood. 1992; 80: 879–886.
[32] Campani D, Esposito I, Boggi U, Cecchetti D, Menicagli M, De Negri F, *et al*. Bcl-2 expression in pancreas development and pancreatic cancer progression. The Journal of Pathology. 2001; 194: 444–450.
[33] Borner C. The Bcl-2 protein family: sensors and checkpoints for life-or-death decisions. Molecular Immunology. 2003; 39: 615–647.
[34] Hengartner MO. The biochemistry of apoptosis. Nature. 2000; 407: 770–776.
[35] Xu C, Zhao H, Chen H, Yao Q. CXCR4 in breast cancer: oncogenic role and therapeutic targeting. Drug Design, Development and Therapy. 2015; 9: 4953–4964.
[36] Teicher BA, Fricker SP. CXCL12 (SDF-1)/CXCR4 pathway in cancer. Clinical Cancer Research: an Official Journal of the American Association for Cancer Research. 2010; 16: 2927–2931.
[37] Kocher F, Puccini A, Untergasser G, Martowicz A, Zimmer K, Pircher A, *et al*. Multi-omic Characterization of Pancreatic Ductal Adenocarcinoma Relates CXCR4 mRNA Expression Levels to Potential Clinical Targets. Clinical Cancer Research: an Official Journal of the American Association for Cancer Research. 2022; 28: 4957–4967.
[38] Liao Z, Ye L, Li T, Jin X, Lin X, Fei Q, *et al*. Tissue-resident CXCR4^{+} macrophage as a poor prognosis signature promotes pancreatic ductal adenocarcinoma progression. International Journal of Cancer. 2023; 152: 2396–2409.
[39] Farren MR, Mace TA, Geyer S, Mikhail S, Wu C, Ciombor K, *et al*. Systemic Immune Activity Predicts Overall Survival in Treatment-Naïve Patients with Metastatic Pancreatic Cancer. Clinical Cancer Research: an Official Journal of the American Association for Cancer Research. 2016; 22: 2565–2574.
[40] Peng PJ, Li Y, Sun S. On the significance of Tim-3 expression in pancreatic cancer. Saudi Journal of Biological Sciences. 2017; 24: 1754–1757.
[41] Pan Y, Gao J, Lin J, Ma Y, Hou Z, Lin Y, *et al*. High-dimensional single-cell analysis unveils distinct immune signatures of peripheral blood in patients with pancreatic ductal adenocarci-

Journal of
BIOLOGICAL REGULATORS
and Homeostatic Agents

noma. Frontiers in Endocrinology. 2023; 14: 1181538.

[42] Waters AM, Der CJ. KRAS: The Critical Driver and Therapeutic Target for Pancreatic Cancer. Cold Spring Harbor Perspectives in Medicine. 2018; 8: a031435.

[43] Ino Y, Oguro S, Yamazaki-Itoh R, Hori S, Shimada K, Hiraoka N. Reliable evaluation of tumor-infiltrating lymphocytes in pancreatic cancer tissue biopsies. Oncotarget. 2019; 10: 1149–1159.

[44] Hou YC, Chao YJ, Hsieh MH, Tung HL, Wang HC, Shan YS. Low $CD8^+$ T Cell Infiltration and High PD-L1 Expression Are Associated with Level of $CD44^+/CD133^+$ Cancer Stem Cells and Predict an Unfavorable Prognosis in Pancreatic Cancer. Cancers. 2019; 11: 541.

[45] Hilmi M, Bartholin L, Neuzillet C. Immune therapies in pancreatic ductal adenocarcinoma: Where are we now? World Journal of Gastroenterology. 2018; 24: 2137–2151.

[46] Kurahara H, Takao S, Maemura K, Mataki Y, Kuwahata T, Maeda K, *et al*. M2-polarized tumor-associated macrophage infiltration of regional lymph nodes is associated with nodal lymphangiogenesis and occult nodal involvement in pN0 pancreatic cancer. Pancreas. 2013; 42: 155–159.

[47] Kurahara H, Shinchi H, Mataki Y, Maemura K, Noma H, Kubo F, *et al*. Significance of M2-polarized tumor-associated macrophage in pancreatic cancer. The Journal of Surgical Research. 2011; 167: e211–e219.

[48] Dallal RM, Christakos P, Lee K, Egawa S, Son YI, Lotze MT. Paucity of dendritic cells in pancreatic cancer. Surgery. 2002; 131: 135–138.

[49] Tjomsland V, Sandström P, Spångeus A, Messmer D, Emilsson J, Falkmer U, *et al*. Pancreatic adenocarcinoma exerts systemic effects on the peripheral blood myeloid and plasmacytoid dendritic cells: an indicator of disease severity? BMC Cancer. 2010; 10: 87.

[50] Hirooka S, Yanagimoto H, Satoi S, Yamamoto T, Toyokawa H, Yamaki S, *et al*. The role of circulating dendritic cells in patients with unresectable pancreatic cancer. Anticancer Research. 2011; 31: 3827–3834.

[51] Hu H, Hang JJ, Han T, Zhuo M, Jiao F, Wang LW. The M2 phenotype of tumor-associated macrophages in the stroma confers a poor prognosis in pancreatic cancer. Tumour Biology: the Journal of the International Society for Oncodevelopmental Biology and Medicine. 2016; 37: 8657–8664.